Nanoscale Advances

ROYAL SOCIETY OF CHEMISTRY

PAPER

View Article Online
View Journal | View Issue

Cite this: *Nanoscale Adv.*, 2025, **7**, 7836

Ion-imprinted carbon dots: rationally designed fluorescent probes for the detection of selected metal ions from aqueous solutions

Aishwarya Joji Mathew, [a] T. P. Vinod *[ab] and Yamuna Nair [a]

Photoluminescence properties of Carbon Dots (CDs) have been leveraged for their use as sensors for a variety of analytes, including inorganic ions, organic molecules, and biomolecules. The selective fluorescence response of CDs to specific analytes is generally not pre-designed. Rationally designed synthesis of CDs with pre-defined selectivity to specific analytes is a less explored avenue. This study presents a novel method for the customized synthesis of CD fluorescent probes and an ion-imprinting-based selective detection of metal ions using these CDs. Poly(sodium 4-styrenesulfonate) [PSS] treated with Cd(II) ions was used as the precursor for preparing Cd-imprinted CDs, and a modified form of these CDs was used for the sensing of Cd(II) in aqueous solutions. As synthesized CDs have Cd(II) ions on their surface, which were subsequently removed through appropriate chemical treatment. This removal results in binding sites of Cd(II) ions on the CDs. Formation of such binding sites results in alterations of the fluorescence of CDs. Exposure of these particles to analytes containing Cd(II) ions leads to the re-occupation of the binding sites by the metal ions, resulting in a distinct fluorescence response, which serves as the sensing readout. Effectiveness of this 'ion-imprinting' approach is demonstrated by the selective and sensitive fluorescence response of the CDs towards Cd(II) ions, with a limit of detection (LOD) of 3.62 nM. This strategy of Cd(II) detection using ion-imprinted CDs represents a novel effort in CD-based sensors, and this can be extended to the sensing of other cations also.

Received 18th September 2025
Accepted 16th October 2025

DOI: 10.1039/d5na00892a

rsc.li/nanoscale-advances

1. Introduction

Carbon dots (CDs) are a unique class of quasi-spherical, zero-dimensional, carbon-based nanomaterials, typically smaller than 10 nm in size, distinguished for their exceptional opto-electronic properties, including strong photoluminescence and tunable fluorescence emission.[1] Properties of CDs can be enhanced/altered through different physical or chemical modification strategies, including doping, surface passivation, self-assembly, controlling the shape and size, composite blending, *etc.*[2] The useful features of CDs that make them ideal functional materials for various applications include tunability of photoluminescence (PL), excellent water solubility, high photostability, low toxicity, low cost, and biocompatibility.[3,4] The primary reason for PL in CDs is believed to be quantum confinement,[5] which leads to the formation of distinct quantized energy levels, leading to the formation of a band gap.[6] CDs are generally synthesized from carbon sources such as organic molecules, polymers, or carbon precursors through simple and cost-effective methods such as hydrothermal treatment and microwave irradiation,[7] following top-down or bottom-up approaches.[8] These nanoparticles possess a high surface area and can be easily functionalized or modified, leading to customized optical properties and chemical behavior.[9]

CDs have emerged as promising candidates as sensing probes owing to their unique optical properties, biocompatibility, and ease of functionalization.[10] Changes in photoluminescence properties of CDs, such as enhancement, quenching, and shift in emission wavelength, in response to the presence of specific species, have been utilized for the detection of various analytes, including inorganic ions, organic molecules, and biomolecules.[11–13] The selective fluorescence response of CDs to specific analytes is not generally pre-designed. Usually, the applicability of a CD system as a sensor is identified from post-synthesis fluorescence studies in a trial-and-error mode. To the best of our knowledge, there are no examples in the literature for the customized synthesis of CDs aimed at their usage as a sensor for a particular analyte. Rationally designed synthesis of CDs with pre-designed selectivity to specific analytes is an avenue worth exploring. Herein, we present the design and synthesis of ion-imprinted CDs and a fluorescence-based method for the detection of Cd(II) ions utilizing these nanoparticles. Poly(sodium 4-styrenesulfonate) [PSS] treated with Cd(II) ions was used as a precursor to prepare Cd-imprinted CDs, which, after modification, were used to

[a]*Department of Chemistry, Christ University, Hosur Road, Bengaluru 560029, India. E-mail: vinod.tp@christuniversity.in*

[b]*Centre for Renewable Energy and Environmental Sustainability, Christ University, Bengaluru 560029, India*

detect Cd(II) ions in aqueous solutions. We demonstrate the potential of this innovative ion-imprinting method in CDs by studying the selective and sensitive fluorescence response for Cd(II) ions in aqueous solutions.

We used the principles of ion-imprinting, which is a technique used to create specific binding sites for the target analyte within a polymer matrix.[14] It involves the template-induced formation of recognition sites that are complementary in shape, size, and functionality to the target species.[15] After removing the template analyte, the resulting imprinted materials exhibit selective recognition and binding affinity towards the target species.[16] This approach is widely employed in various applications, including sensing, separation, catalysis, and drug delivery, offering advantages such as high selectivity, stability, and reusability compared to other methods.[17,18] Although ion -imprinting in polymers is well-studied,[19,20] ion-imprinting on CDs is not reported to the best of our knowledge.

In this work, we employed CDs as substrates for imprinting metal ions to create a highly efficient, rapid, selective, and sensitive metal ion sensor. The CDs, modified with the targeted metal ions, were derived from the polyelectrolyte poly(sodium 4-styrenesulfonate) [PSS]. The ion-imprinting method reported here involves three straightforward steps that ensure high selectivity for the sensing of a specific metal ion. We explore and propose the mechanism that manifests this specificity and demonstrate the method's effectiveness in detecting Cd(II) ions.

2. Experimental

2.1 Chemicals

Quinine sulphate (QS), poly(sodium 4-styrenesulfonate) [PSS], $FeCl_2$, $CdCl_2$, $MgCl_2$, $HgCl_2$, $FeCl_3$, Li_2SO_4, $CaCl_2$, $ZnCl_2$, NaCl, $PbNO_3$, $CuSO_4$, $NiSO_4$, NaOH, KCl, $Na_2HPO_4 \cdot 12H_2O$, and NaH_2PO_4 were procured from Sigma-Aldrich. Ethanol and acetone were supplied by Thomas Baker (Chemicals) Pvt Ltd. Syringe filters with pore sizes of 0.44 μm and 0.22 μm were procured from Sigma-Aldrich. Dialysis Membrane-70 with a molecular weight cutoff ranging from 12 000 Da to 14 000 Da and Whatman 40 filter papers with a size of 12.5 cm were purchased from Future Lab, India.

2.2 Synthesis of PSS-CDs tethered with Cd(II) ions

(0.18 g) of PSS (Mw ~70 000) and (0.018 g) of $CdCl_2$ were mixed in 40 mL of deionized water. The homogeneous solution was moved to a Teflon-lined autoclave (stainless steel) and heated in a hot air oven for 14 hours at 160 °C. After cooling to room temperature, the solution was filtered through a syringe filter, and the filtrate was dialyzed for 24 hours. The resulting PSS-Cd-CDs (with the concentration of 0.082 g ml^{-1}) were stored at 4 °C for further studies. PSS-Cu-CDs and PSS-Hg-CDs were also synthesized using similar procedures, using $CuSO_4$ and $HgCl_2$, respectively.

2.3 Creation of binding sites in PSS-Cd-CDs

The PSS-Cd-CDs solutions were mixed with an equal volume of 1 M NaOH and allowed to stand for 2 hours to precipitate Cd $(OH)_2$. The resulting PSS-Cd-CDs with binding sites were then collected by syringe filtration, and the filtrate was dialysed for 24 hours and was used for subsequent studies. Cu(II) ions and Hg(II) ions from PSS-Cu-CDs and PSS-Hg-CDs were also removed in same manner resulting in PSS-Cu-CDs with the binding sites and PSS-Hg-CDs with the binding sites, respectively.

2.4 Characterizations

The high-resolution transmission electron microscopy (HRTEM) images were taken using the JEOL JEM-2100 with a LaB6electron gun, that operated at 200 kV. X-ray Photoelectron Spectroscopy (XPS) analysis was performed on a PHI 5000 Versa Prob II, FEI Inc. The absorbance measurements were taken on the Shimadzu UV-1500 spectrophotometer, and photoluminescence (PL) measurements were made on the Shimadzu RF 6000 spectrofluorometer. The measurements of PL lifetime were conducted using the JOBIN-VYON M/S fluorocube system. Inductively coupled plasma-optical emission spectral (ICP-OES) analysis was carried out with the Avio 200 model from PerkinElmer (spectral range: 165–900 nm), with the concentrations of standard ranging from 1.25 to 20 ppm (ICP multi-element standard solution IV). Atomic absorption spectrophotometer measurements were obtained using a Shimadzu AA-6880 atomic absorption spectrophotometer, with the concentration of standards ranging from 0.05 to 0.2 ppm. The zeta potential was measured using Dynamic Light Scattering (DLS) with a zetasizer (ZS90) instrument. The SEM images were obtained utilizing the Thermo Scientific Apreo S LoVac, with a maximum accelerating voltage of 30 kV. A Shimadzu IR Spirit spectrophotometer in a frequency range of 4000–500 cm^{-1} with a spectral resolution of 4 cm^{-1} was utilized to record Fourier Transform Infrared Spectroscopy (FT-IR) analysis. The X-ray diffractometer analysis was carried out using the Bruker D8 advance instrument with Cu-Kα radiation (wavelength: 1.5406 Å) under operating conditions of 40 kV and 20 mA. The Raman spectra were recorded using an INVIA instrument (England) with a 514 nm argon ion laser, over the spectral range of 100–4000 cm^{-1}. ^{1}H NMR spectra of PSS and PSS-Cd-CDs were obtained using a Bruker solution state spectrometer (600 MHz). The pH of PSS-Cd-CDs dispersions was measured using a pHep + Waterproof Pocket pH Tester (HI98108), which has a resolution of 0.01 pH.

2.5 ^{1}H NMR characterization of PSS and PSS-Cd-CDs

PSS-Cd-CDs were freeze-dried to obtain powdered PSS-Cd-CDs. PSS and PSS-Cd-CDs were dissolved in deuterium oxide (99.9%) for the analysis. The prepared solutions were transferred into a 5 mm NMR tube, and the ^{1}H NMR spectra of PSS and PSS-Cd-CDs were acquired using an NMR spectrometer. The resulting.spectral data were processed and analysed using MestReNova software and plotted using Origin software.

2.6 Quantum yield calculations

The Quantum Yield (QY) of PSS-Cd-CDs was estimated using the equation mentioned below. In eqn (1), 'st' denotes the reference standard (quinine sulphate), and 'x'relates' to PSS-Cd-CDs. The

QY of reference standard (quinine sulphate) in (0.1 M) H_2SO_4 is 54%.[21] In this equation, η represents the refractive index of the solvent (water), A denotes the absorbance, Q denotes the quantum yield, while I indicates the fluorescence intensity, with the excitation wavelength of 260 nm.

$$Q_x = Q_{st} \cdot \frac{A_{st}}{A_x} \cdot \frac{I_x}{I_{st}} \cdot \left(\frac{\eta_x^2}{\eta_{st}^2}\right) \quad (1)$$

2.7 Detection of Cd(II)

The Cd(II) ion solutions were prepared using a phosphate buffer of pH 7.0. The detailed procedure for the detection is as follows:

A measured volume (20 μL) of the aqueous dispersion of CDs of Stage 2 was added to 3 mL of phosphate buffer solution, followed by different volumes of 10^{-5} M concentrations of the Cd(II) solutions. The PL spectra were recorded after incubating at room temperature for 5 minutes. The concentration of CDs at all three stages was made identical by adjusting their optical density to the same value.

2.8 Analysis of real samples

The practical application of the CDs of Stage 2 was tested through selective and sensitive detection of Cd ions in tap water (collected from Christ University, Bangalore, India) and lake water (collected from Begur lake, Bangalore, India), which were filtered using a 0.22 μm membrane. In brief, 3 mL of real samples was spiked with 20 μL of different concentrations of Cd(II) ions (10, 20, 30, 40, and 50 μM, respectively). To each of these analyte solutions, 20 μL of Stage 2 CDs was added, and the fluorescence was recorded with excitation using a 260 nm wavelength.

3. Results and discussion

3.1 Experimental design

The ion-imprinting method involves three stages of Cd–CD interactions and capturing of the corresponding fluorescence responses (Fig. 1). Cd(II) tethered CDs were prepared through the hydrothermal treatment of poly(sodium 4-styrenesulfonate) [PSS] in the presence of Cd ions (Stage 1), and the product is indicated as PSS-Cd-CDs. Cd ions tethered to the CDs were then removed using NaOH, creating binding sites for these metal ions in the CDs (Stage 2). When these CDs were treated with an analyte solution containing Cd(II) ions, the binding sites were refilled with the Cd ions (Stage 3). The detection strategy involves analysing the fluorescence response at all three stages. CDs without the metal ions (PSS-CDs) were also prepared and tested as a control sample.

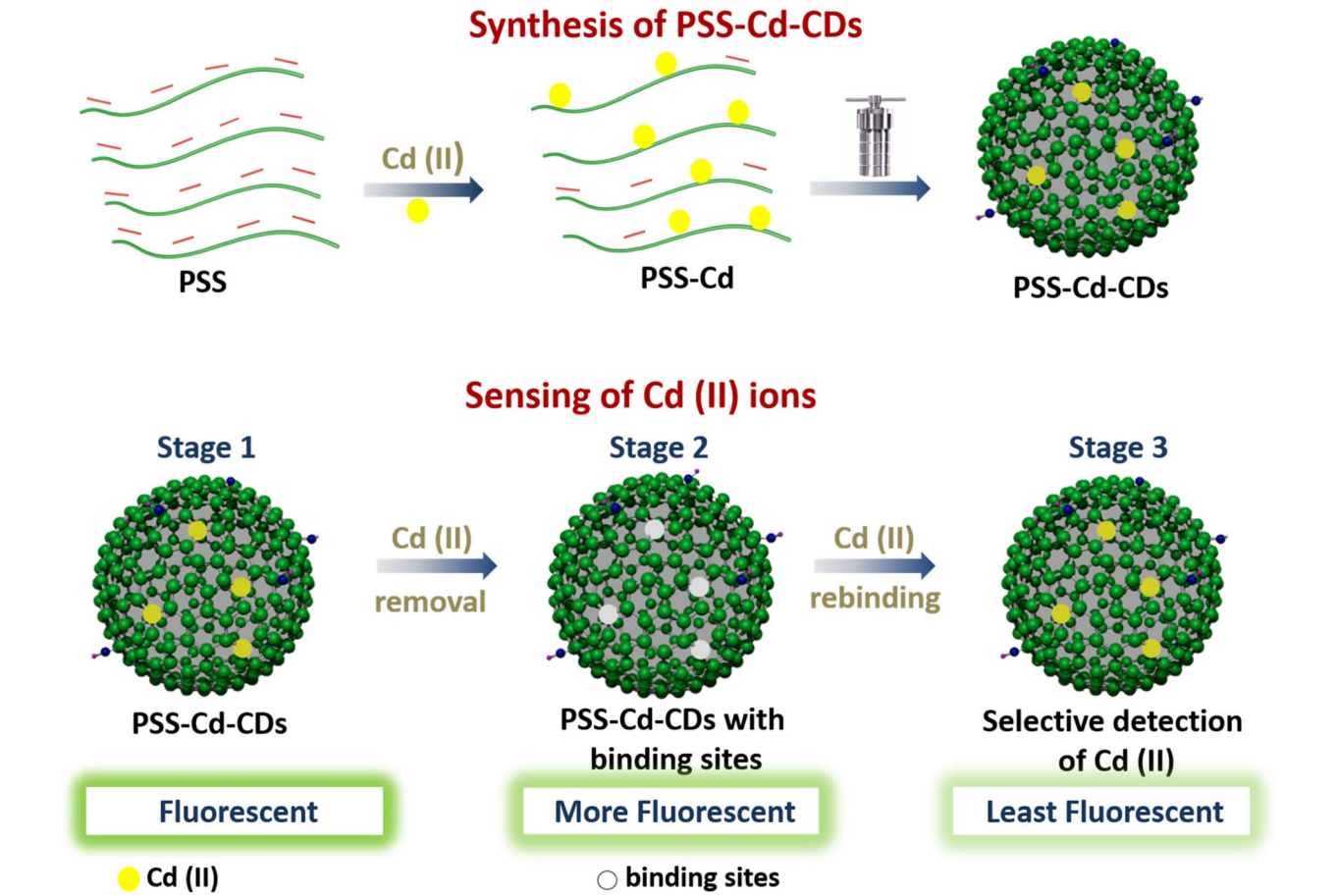

Fig. 1 Schematic representation (not in scale) of the ion-imprinting strategy for Cd(II) ion sensing.

In the precursor solution containing the polyelectrolyte PSS and Cd ions, Cd(II) ions are attracted to the negative charges on the PSS chain through electrostatic forces. CDs prepared from the hydrothermal treatment of this precursor solution have Cd ions tethered to the nanoparticle surface. In Stage 2, these metal ions are removed using NaOH, leaving behind PSS-Cd-CDs with binding sites. In Stage 3, when these PSS-Cd-CDs with binding sites are exposed to an analyte solution containing Cd ions, they are expected to show a specific and selective fluorescence response. The specificity and selectivity result from the analyte ion's capability to establish coordinate bonds[22] with the oxygen functionalities on the surface of CDs, which is influenced by factors such as ionic radius, coordination number, and charge.[23]

3.2 Characterization of the PSS-Cd-CDs system

HRTEM images and size distribution histogram showed that the PSS-Cd-CDs had a quasi-spherical shape and a mean diameter of 5.56 nm (Fig. 2a and b). The morphology of these CDs remains unchanged while going through the next two stages, namely removal (Stage 2) and rebinding (Stage 3) (Fig. S1 and S2, SI). The lattice fringes observed from the HRTEM images, with an interplanar spacing of 0.24 nm, correspond to the (100) plane of the graphitic carbon, confirming the structural identity of the PSS-Cd-CDs (Fig. 2c).[24] The PSS-Cd-CDs were found to be partially crystalline, with lattice fringes visible only in certain domains. The SAED pattern of PSS-Cd-CDs, showing diffused rings, indicates their polycrystalline nature (Fig. 2d).[25] Similarly, HRTEM images and the size distribution histogram of PSS-CDs were also analysed as a control sample. These analyses revealed the formation of PSS-CDs with a mean diameter of approximately 3.70 nm (Fig. S3, SI) and an interplanar spacing of 0.21 nm corresponding to the (100) plane of the graphitic carbon.

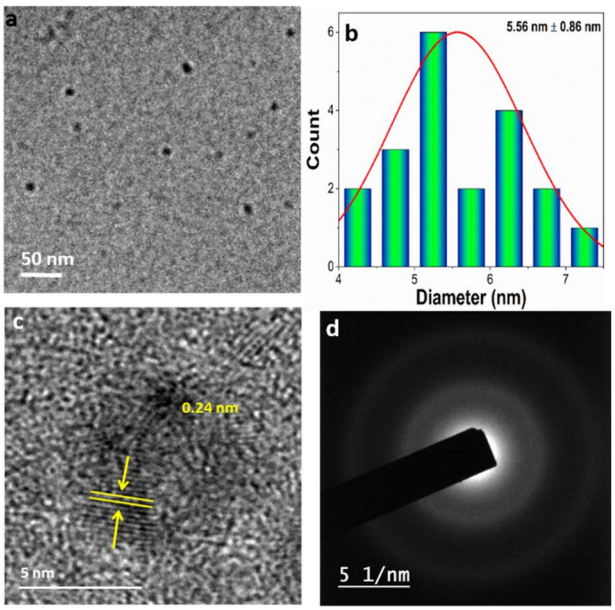

Fig. 2 (a) TEM image, (b) histogram depicting the size distribution, (c) HRTEM image, and (d) SAED pattern of PSS-Cd-CDs.

The optical properties of PSS-Cd-CDs are depicted in Fig. 3. UV-visible absorbance spectrum was recorded to analyze the electronic transitions occurring in the CDs. The spectrum displays peaks at 220 nm and 260 nm, which can be attributed to π–π* transitions of the conjugated C=C bond and n–π* transitions of the C=O bonds present in PSS-Cd-CDs (Fig. 3a). Similar electronic transitions were observed for CDs in all the three stages of experiments (Fig. 3d). PSS-CDs also exhibited two peaks at 220 nm corresponding to π–π* transitions and 260 nm corresponding to n–π* transitions (Fig. S4a, SI). These transitions results from the graphitic cores and surface defects of CDs.[26] The PSS-Cd-CDs exhibited bright green fluorescence under irradiation by UV light (λ_{ex} = 254 nm). In day light, solution of PSS-Cd-CDs was observed to have a pale-yellow colour (Fig. S5, SI). In the emission spectra of PSS-Cd-CDs, the maximum emission is recorded at 315 nm when excited with a wavelength of 260 nm (Fig. 3b). Similar emission spectra were observed for PSS-CDs (Fig. S4b, SI). The PSS-Cd-CDs exhibits excitation wavelength dependent emissions at different excitation wavelengths ranging from 220 to 400 nm taken at the interval of 20 nm. The PSS-Cd-CDs exhibit maximum emission (λ_{max}) at 315 nm upon excitation at 260 nm (Fig. 3c). Similarly, for PSS-CDs, the maximum emission occurs at 315 nm when excited at 260 nm (Fig. S4c, SI). The QY for PSS-Cd-CDs is determined to be 21.2%. The quantum yield depends upon the surface defects and functional groups of the CDs.[27] The fluorescence response of the three stages involved in the usage of the PSS-Cd-CD system for Cd(II) ion detection was recorded (Fig. 3e). The fluorescence observed in Stage 3 was much lower than that in Stages 1 and 2, which is in accordance with the proposed mechanism. The fluorescence lifetime for PSS-Cd-CDs (Stage 1) is estimated to be 1.836 ns after fitting the decay curve with single exponential function (Fig. 3f). The fluorescence life time of Stage 1 (PSS-Cd-CDs) is larger compared to PSS-CDs (Fig. S4d, SI). This increased PL lifetime is mechanistically linked to passivated defects on the surfaces of the CDs, effectively acting as traps for excitation energy.[28] The fluorescence lifetime of Stage 3 was found to be shorter than that of Stage 2 (Table 1). This shows that the addition of analyte Cd(II) ions to the Stage 2 CDs decreases the fluorescence lifetime.[29] The fluorescence lifetime results suggest that the quenching of fluorescence of CDs at Stage 3 is caused by Cd ions, presumably due to electron transfer from the excited state of CDs of Stage 2 to the Cd(II) ions.[29] The stability of Stage 2 CDs under different conditions, including storage, pH, and KCl concentration was studied and the results are presented in Fig. S6, SI. Fig. S6a, SI, illustrates the influence of ionic strength on the PL intensity of Stage 2 CDs. A significant decrease in PL intensity is observed with increasing KCl concentration, which is attributed to the aggregation of particles, which is induced by the higher salt content.[3] A reduction in emission intensity is observed under acidic conditions. At higher pH, however, deprotonation of functional groups and the presence of structural defects lead to an enhancement in the PL intensity of Stage 2 CDs (Fig. S6b, SI).[4] The Stage 2 CDs show a decrease in PL,

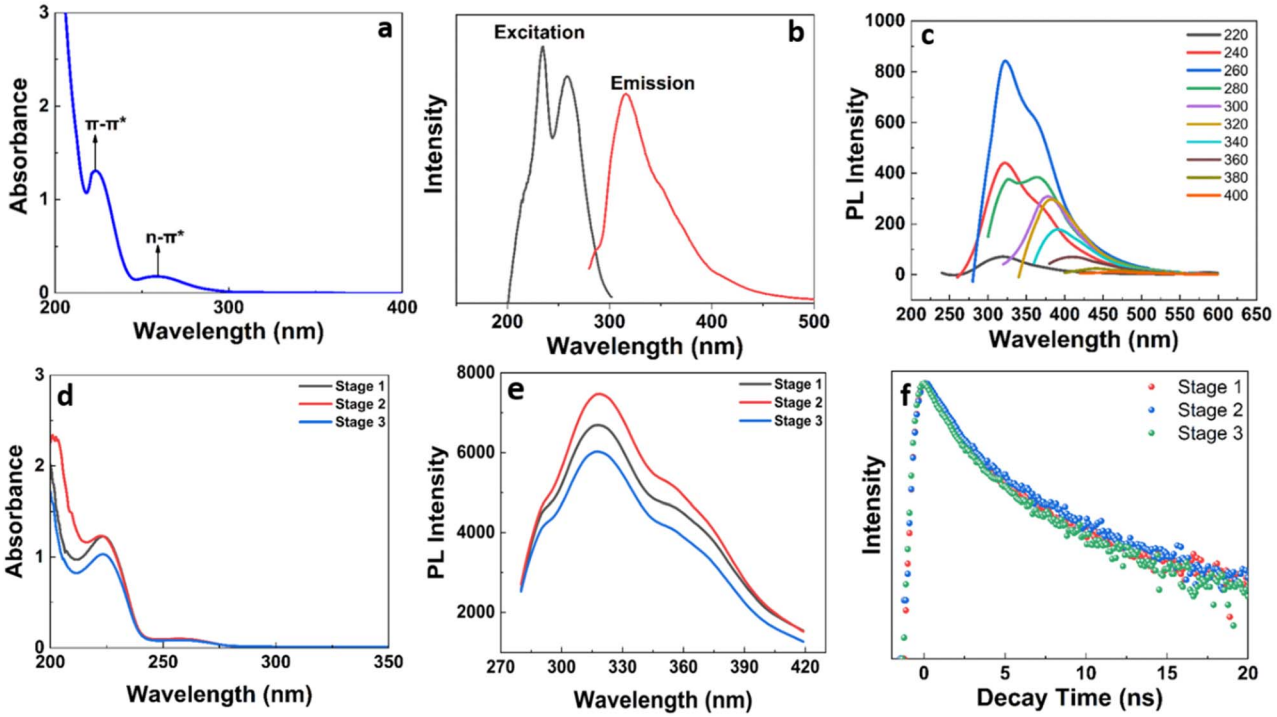

Fig. 3 (a) UV-visible absorption spectra, (b) excitation spectrum (emission recorded at 315 nm) and emission spectrum (λ_{ex} = 260 nm), (c) excitation dependent emissions of PSS-Cd-CDs, (d) UV-visible absorption spectra of carbon dots in three stages, (e) the fluorescence response of carbon dots at various stages of the experiment, and (f) fluorescence lifetime of carbon dots at various stages.

Table 1 Average fluorescence lifetime of all three stages of the experiment

Sl no.	Samples	Average life time [ns]
1	PSS-CDs	1.393
2	Stage 1	1.836
3	Stage 2	2.721
4	Stage 3	1.451

with only a 4.9% drop after one month of storage and a 15.2% reduction after six months (Fig. S6c, SI). This decline in photostability is attributed to the aggregation behaviour of CDs of Stage 2.[4] These observations indicate that the Stage 2 CDs are stable under various conditions.

The PL properties of the aqueous suspensions of PSS-CDs (control), PSS-Cd-CDs (Stage 1) and CDs of Stage 2 (Fig. 4a) in the presence of numerous metal ions such as Ca(II), Cd(II), Cu(II), Fe(II), Fe(III), Hg(II), Li(II), Pb(II), Mg(II), Na(I), Ni(II), Zn(II) were studied under the same conditions. The fluorescence studies revealed that the quenching response of Stage 2 CDs towards Cd(II) was more effective compared to the quenching response of PSS-CDs and PSS-Cd-CDs towards Cd(II) ions (Fig. 5a and c).[30] The fluorescence quenching of CDs of Stage 2 (40.2% upon the addition of 20 μL of Cd(II)) was found to be highly selective to Cd ions. Thus, it is evident that the Cd(II) ions can strongly bind to CDs of Stage 2, leading to significant fluorescence quenching. Other metal ions showed contrasting responses, probably because they do not fit the recognition sites, making them incapable of quenching the fluorescence of CDs of Stage 2, even though they can still interact with CDs of Stage 2 through hydrogen bonding. This indicates that the binding sites have been created on the surface of CDs of Stage 2, and the binding sites are being filled selectively by the Cd(II) ions. This observation suggests that the spectral selectivity of Stage 2 CDs is significantly more towards Cd(II) by the creation of specific recognition sites. These observations confirm the specific affinity of the CDs of Stage 2 for Cd ions, which is attributed to both the binding sites and the effectively designed imprinted cavities tailored for Cd ions.

The PL studies were conducted for the mixture of Stage 2 CDs and selected set of metal ions (with and without Cd(II) ions) (Fig. 6a). The fluorescence studies were also conducted for (i) Stage 2 CDs with various metal ions and Cd(II) ions, and (ii) Stage 2 CDs with Cd(II) ions alone (Fig. 6b). From both the studies, it was confirmed that the quenching is selectively due to Cd(II) ions. This data further verifies the exceptional specific interaction of the CDs of Stage 2 for Cd(II) ions, primarily attributable to the specific binding interactions and the custom-designed imprinted cavities that accommodate Cd(II). From the above studies, CDs of Stage 2 were found to be capable of the selective detection of Cd(II), which makes it a potential candidate for a fluorescent probe based on an ion-imprinting strategy.

The fluorescence intensity of CDs of Stage 2 exhibited a linear quenching response as the Cd(II) concentration varied within the range of 0–160 nM (Fig. 4b). With an increase in the concentration of Cd ions, CDs of Stage 2 resulted in substantial

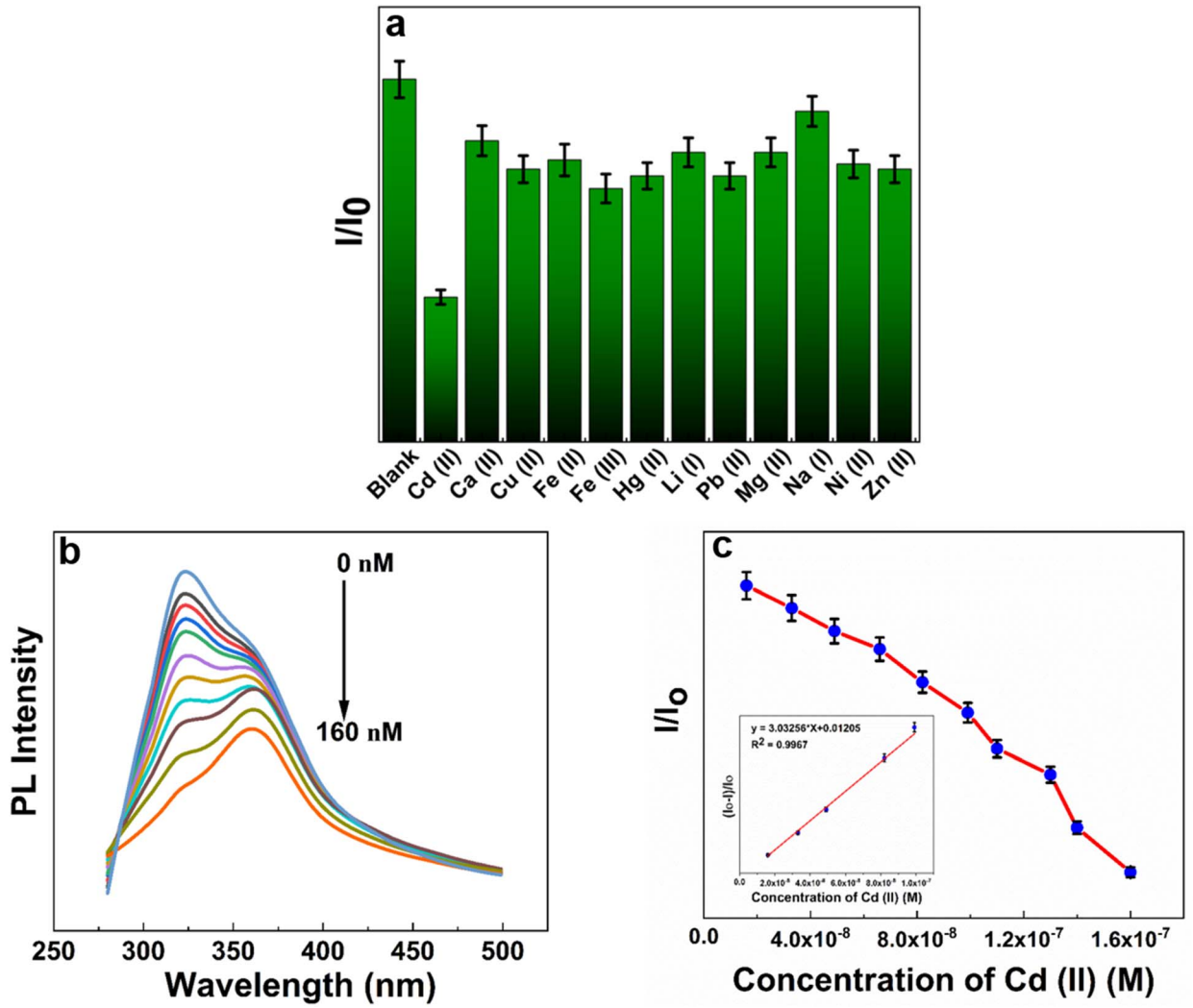

Fig. 4 (a) The PL response of CDs (Stage 2) to various metal ions, (b) The PL spectra of Stage 2 CDs exposed to various concentrations of Cd(II) (λ_{ex} = 260 nm), and (c) the plot of I/I_O *versus* the Cd ion concentrations, with the fitted linear plot at lower concentrations shown in the inset.

quenching of their fluorescence.[31] The photoluminescence intensity decreases linearly with increasing concentrations of Cd ions up to 160 nM. Beyond this concentration, the extent of fluorescence quenching minimizes as the surplus Cd(II) ions do not fully interact with the CDs of Stage 2. There was no substantial quenching observed for PSS-CDs and PSS-Cd-CDs, while the concentration of Cd was varied within the range of 0–160 nM (Fig. 5b and d). To assess the sensitivity of Stage 2 CDs towards Cd(II) ions, fluorescence response was recorded by varying the concentration of Cd ions. Stage 2 CDs showed exceptional sensitivity towards Cd ions, even at low concentrations of Cd ions. The imprinting factor (IF) serves as a measure for assessing the imprinting effect, selectivity, and affinity of a metal ion towards imprinted material. (In ion-imprinted polymers, the IF is defined as the ratio of the Stern–Volmer constant of ion-imprinted polymer (K_{SV}, IIP) to non-ion-imprinted polymer (K_{SV}, NIP), which is used to compare the selectivity and affinity of an ion between the ion-imprinted polymer (IIP) and non-ion-imprinted polymer (NIP)).[32] In our study, CDs of Stage 2 can be considered as IIP and PSS-CDs as NIP, the K_{SV} for the CDs of Stage 2 (Fig. 4c) and PSS-CDs (Fig. S7a, SI) were calculated using the Stern–Volmer plot and were found to be 3.032 and 1.123, respectively. The IF for our study was calculated by determining the ratio of K_{SV} of CDs of Stage 2 to K_{SV} of PSS-CDs and was found to be 2.699. This indicates the selective recognition of Cd ions for Stage 2 CDs, and it enhances the quenching efficiency and sensitivity of CDs of Stage 2. To examine the binding affinity of Cd ions to CDs of Stage 2, we performed an analysis using Job's plot, monitoring absorbance variations across different Cd(II) ion concentrations.[33] Using Job's plot, we determined the binding ratio of CDs of Stage 2 to Cd(II) ions to be 1 : 1, as illustrated in Fig. S7b, SI. Furthermore, the binding constant (K_b) was determined by evaluating the ratio of the intercept to the slope, derived from the Bansi–Hildebrand (B–H) plot, as depicted in Fig. S7c, SI. The B–H plot shows the binding efficiency of Cd(II) ions with the CDs of Stage 2 to be 1.45 × 10^6 M^{-1}, highlighting the strong binding affinity and selectivity of CDs of Stage 2 specifically for

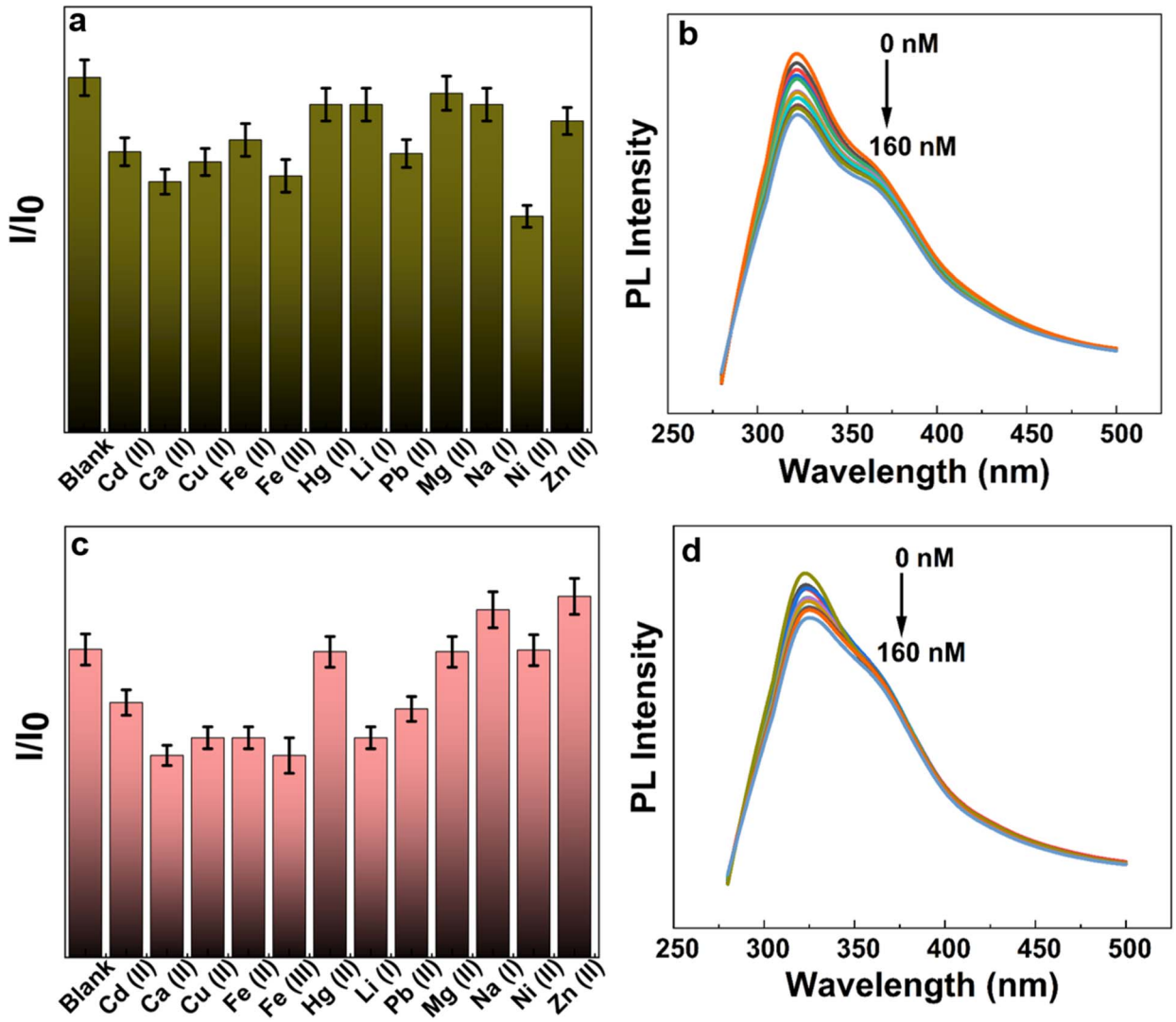

Fig. 5 PL measurements from control samples. (a) The PL intensity at 315 nm of PSS-CDs in response to different metal ions, (b) the PL spectra of PSS-CDs exposed to various concentrations of Cd ions (λ_{ex} = 260 nm), (c) the fluorescence intensity at 315 nm of PSS-Cd-CDs (Stage 1) in response to numerous metal ions, and (d) the fluorescence spectra of PSS-Cd-CDs exposed to different concentrations of Cd(II) (λ_{ex} = 260 nm).

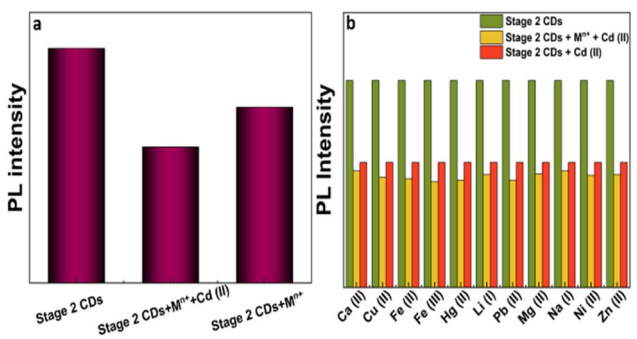

Fig. 6 (a) The photoluminescence spectra of CDs of Stage 2 in response to the mixture of metal ions (Ca(II), Cu(II), Fe(II), Fe(III), Hg(II), Li(II), Pb(II), Mg(II), Na(I), Ni(II), and Zn(II)), both in presence and absence of Cd(II) ions, and (b) the PL intensity at 315 nm of CDs of Stage 2 with other metal ions added with Cd(II) ions, and Cd(II) ions alone in CDs of Stage 2 respectively.

Cd(II) ions. This analysis highlights the significant interaction and binding capabilities of Stage 2 CDs toward Cd ions. To investigate the fluorescence quenching efficiency of Stage 2 CDs by Cd(II), the Stern–Volmer equation was used.[34] The PL quenching of Stage 2 CDs follows the Stern–Volmer equation, demonstrating a linear relationship between the parameters $I_0 - I/I_0$ and Cd(II) ion concentration. The CDs of Stage 2 showed a linear correlation coefficient (R^2) of 0.9967 for the Cd(II) ions with the quenching constant (K_q) calculated to be 3.0325×10^{14} M^{-1}. The detection limit of Cd(II) by CDs of Stage 2 is calculated to be 3.62 nM using the Stern–Volmer equation (Fig. 4c). During the synthesis of Stage 2 CDs, specific recognition sites were created that are complementary in size, shape, and spatial characteristics to the Cd(II) ion template.[22] As a result, Cd(II) ions are more effective at occupying these sites compared to other ions. The presence of Cd ions in the imprinted sites lead to significant quenching in the fluorescence intensity of Stage 2 CDs.

Efficiency of the ion-imprinted PSS-Cd-CDs for detecting Cd(II) ions was compared with previously reported works, which used ion-imprinted polymers along with regular CDs to constitute the sensing system (Table S1). The ion-imprinting strategy we used is novel, versatile, possesses rapid detection capability, and offers the advantage of simplicity and customized selectivity of sensing. In contrast, ion-imprinting in polymers involves multiple functional components and complex approaches, with polymerization and crosslinking agents used for the ion-imprinting methodology. These processes also utilize complex routes and techniques for removal of the metal ions imprinted on the polymers, whereas the strategy used in this work follows a very simple method for the removal of metal ions imprinted on CDs using a simple eluting solvent. Ion-imprinting in carbon dots for fluorescence-based detection of heavy metal ions facilitates higher selectivity, sensitivity, and faster response time, as compared to other existing methods. The literature data presented in Table S1 allowed us to conclude that although the LOD value of our system is higher, it follows a simple approach towards the selective detection of Cd(II) ions.

X-ray photoelectron spectroscopy (XPS) was utilized for validating our hypothesis of the selective binding of Cd ions in custom-made binding sites in Stage 2 CDs. The functional groups of CDs at the three different stages were found to be intact when analysed using XPS (Fig. 7a–l). The XPS survey spectrum of PSS-Cd-CDs revealed the presence of carbon, oxygen, and cadmium contents of 71.60%, 28.40%, and 5.5%, respectively (Fig. 7a). The deconvoluted C (1s) spectra indicated peaks associated with C–C/C=C (284.01 eV) and C–O (285.09 eV) (Fig. 7d). Meanwhile, the analysis of O (1s) revealed the

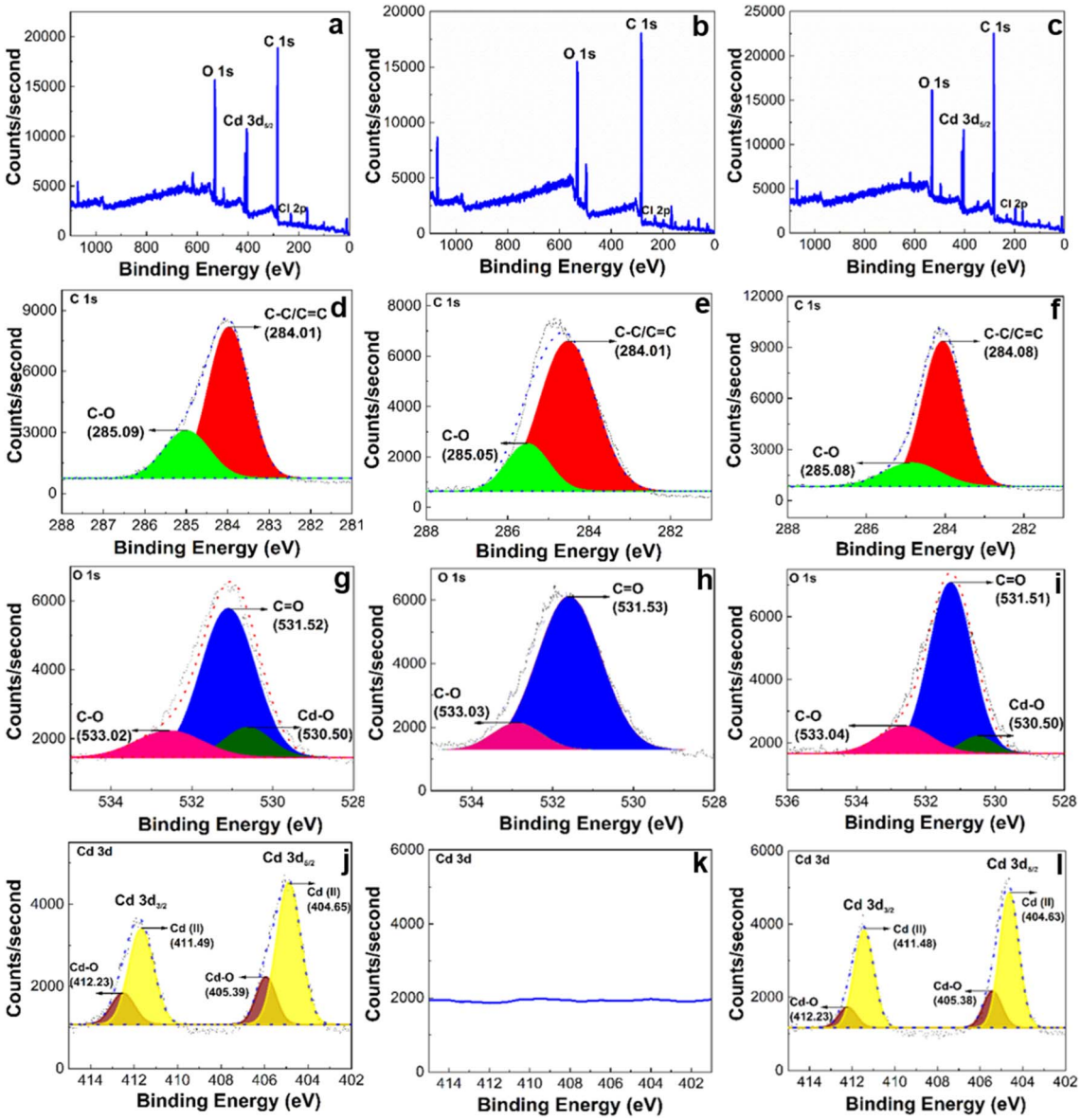

Fig. 7 (a–c) The XPS survey spectrum of Stage 1, Stage 2, and Stage 3 CDs respectively, (d, g and j) deconvoluted XPS spectra of elements of Stage 1 CDs, (e, h and k) deconvoluted XPS spectra of elements of Stage 2 CDs, and (f, i and l) deconvoluted XPS spectra of elements of Stage 3 CDs of the ion-imprinting process.

presence of Cd–O (530.50 eV), C=O (531.52 eV) and C–O (533.02 eV) (Fig. 7g).[4] Two peaks at 404.6 eV and 411.4 eV from the high-resolution spectrum of Cd 3d correspond to the characteristic binding energy of Cd $3d_{5/2}$ and Cd $3d_{3/2}$. The deconvolution of Cd $3d_{5/2}$ gives two peaks corresponding to free Cd ions (404.6 eV) and Cd–O (405.4 eV). Similarly, the deconvolution of Cd $3d_{3/2}$ corresponds to two peaks for free Cd ions (411.4 eV) and Cd–O (412.2 eV) (Fig. 7j). The presence of Cd ions on PSS-Cd-CDs (Stage 1) is ascertained from this data. The XPS recorded 37.83% and 36.18% of carbon and oxygen content, respectively, for PSS-CDs (Fig. S8, SI).

The XPS analysis of the three stages of the imprinting process was conducted to confirm the presence or absence of Cd ions at various stages and to assess the atomic concentration in percentage. The XPS instrument was unable to detect Cd(II) in step 2 (Fig. 7k). Thus, XPS analysis clearly indicated the existence of Cd(II) ions in Stages 1 and 3, whereas in Stage 2, Cd(II) ions were absent. The atomic concentration percentages of the elements found in these samples are listed in Table 2.

The SEM-EDS analysis was performed to examine the chemical composition of CDs during all three stages of ion-imprinting. This analysis was performed to confirm the removal of Cd ions from the surface of CDs and re-binding occurring on the surface of CDs of Stage 2 by Cd(II) ions. The elemental composition of CDs at all the three stages of ion-imprinting was analysed through SEM-EDS (Fig. S9–S11, SI). The data obtained supports the hypothesis about the interactions of CD–Cd(II) ions. Data in Table 3 clearly indicate the presence of Cd(II) ions in Stage 1, the removal of Cd ions in Stage 2, and the re-binding of Cd(II) ions occurring in Stage 3.

To further confirm the presence of Cd ions on the CDs surface, the Inductively Coupled Plasma Optical Emission Spectrometry (ICP-OES) analysis was carried out (Table 4). The ICP-OES analysis affirmed the presence of Cd(II) ions in Stages 1 and 3. The presence of Cd(II) ions in Stages 1 and 3 was re-confirmed through AAS analysis, and the results were comparable to the outcomes of the XPS analysis (Table 5). To understand the process of metal ion binding on the surface of the CDs of Stage 2, where the binding sites are being created, time-dependent AAS study was conducted for 10 minutes (Fig. 8). Time-dependent AAS study was conducted by measuring the concentration of Cd ions present on the surface of Stage 2 CDs at different durations. To conduct this time-depended AAS study, 20 μL of the Cd ions were added to 3 ml of CDs of Stage 2, where binding sites were present, and with the duration of time, the concentration of Cd ions present on the surface of Stage 2 CDs was analysed. From Fig. 8, it is evident that in the first minute, the concentration of Cd ions present on the Stage 2 CDs surface was higher, since the Cd ions gradually started to bind to the surface of the CDs of Stage 2. As the time increased, the concentration of Cd ions found on the surface of the CDs of Stage 2 decreased and became almost constant, which implies that all the binding sites created on the surface of the CDs of Stage 2 are being occupied/re-bonded with the Cd ions. The qualitative analysis test for Cd(II) was carried out by passing the H_2S solution to Stage 1, Stage 2, and Stage 3 CD solutions. Fig. S12, SI clearly indicates the presence of Cd(II)

Table 2 The atomic concentration of elements present in the samples during the three stages of the ion-imprinting process

	Atomic concentration [%]		
Elements	Stage 1	Stage 2	Stage 3
C 1s	65.71	69.34	67.33
O 1s	19.12	21.0	19.81
Cd $3d_{5/2}$	5.5	0	3.4
Cl 2p	1.03	1.34	3.89

Table 3 The EDS data of Cd ions at Stages 1, 2, and 3 of the ion-imprinting process

	Stage 1	Stage 2	Stage 3
Weight %	16.38	0.00	11.49
Atomic %	2.74	0.00	1.77
Atom % error	± 0.29	± 0.00	± 0.34

Table 4 The concentration of Cd(II) ions obtained from the ICP-OES analysis

Sl no.	Samples	Cd(II) [ppm]
1	Stage 1	278.7 ± 1.33
2	Stage 2	Below detectable limit (detection limit = 1 ppm)
3	Stage 3	176.2 ± 1.04

Table 5 The concentration of Cd(II) obtained from the AAS analysis

Sl no.	Samples	Absorbance	Cd(II) [ppm]
1	Stage 1	1.485	0.753 ± 0.0023
2	Stage 2	0.129	0.065 ± 0.0040
3	Stage 3	1.207	0.611 ± 0.0029

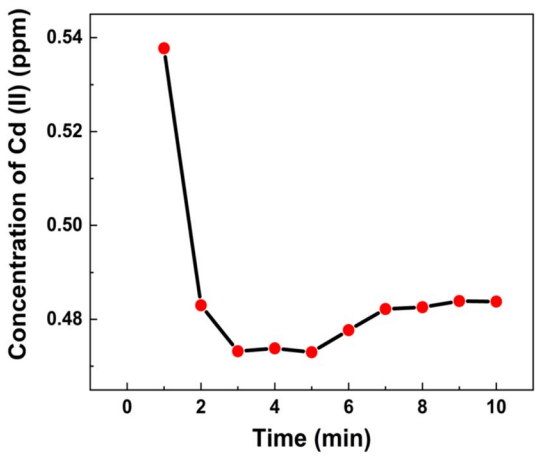

Fig. 8 The time dependent AAS study *versus* the Cd ions concentration present on the surface of the Stage 2 CDs.

ions in Stages 1 and 3 and the absence of these ions in Stage 2, which is in accordance with the proposed mechanism.

The zeta potential values of all three stages of the analysis are shown in Fig. S13, SI. Zeta potential value for Stage 1 CDs was found to be −25.9 mV. The zeta potential value of Stage 2 CDs (−33.5 mV) clearly indicates the removal of Cd(II) ions from the surface of the PSS-Cd-CDs with the increase in the negative zeta potential value compared to Stage 1 CDs. As the Cd ions are removed from the PSS-Cd-CDs surface, the negative charges on the surface of the CDs of the Stage 2 increase. The zeta potential value at CDs of Stage 3 was found to be −26.3 mV, which shows the rebinding of Cd ions to the binding sites formed at Stage 2 CDs. The zeta potential values of all three stages of the analysis show the efficacy of the Cd ions imprinting on PSS-CDs.

FT-IR spectroscopy was used to analyse the functional groups present on the PSS-Cd-CDs surface. FT-IR analysis revealed a band at 3321 cm^{-1}, corresponding to the symmetrical stretching of the –OH functional group, with peak broadening attributed to hydrogen bonding.[35] Furthermore, the presence of C=C stretching at 1638 cm^{-1}, C–C=O stretching at 2115 cm^{-1}, and C–H bending at 1533 cm^{-1} in PSS-Cd-CDs confirms the existence of both carbonyl and alcohol functional groups in it (Fig. 9a). The presence of all these functional groups was intact through all three stages of ion-imprinting. The PSS-CDs also possessed C–C=O, C=C, C–H, and O–H functionalities on their surface, which were confirmed through FT-IR analysis (Fig. S14a, SI). The FT-IR spectra of PSS show a peak at 1139 cm^{-1} corresponding to asymmetric stretching and another one at 1010 cm^{-1} corresponding to symmetric stretching of S=O bonds within sulphonyl groups. Absence of these peaks in PSS-CDs and different stages of CDs indicates that there is no free (unreacted) PSS in the samples (Fig. S14a, SI). The CDs synthesized demonstrated high hydrophilicity and excellent dispersion in water, attributed to the presence of polar functional groups on their surface.[36]

The crystal structure of the CDs was studied using XRD. The diffraction peak in the XRD analysis at 23.15° is associated with (002) facet of graphite (Fig. 9b). The weak peak at 45.72° originated from the in-plane diffraction of graphene-like structured CDs, corresponding to the (101) plane.[37] The broadness of the peak shows partial graphitization and the small size of the CDs.[38] Additionally, the synthesized PSS-Cd-CDs were found to be amorphous in nature, indicated by the reduced intensity and the broader full-width at half maximum in the displayed spectra.[39] The interlayer spacing (d) of PSS-Cd-CDs was calculated to be 0.383 nm. The XRD plot of PSS-CDs also exhibits a diffraction peak at 23.15°, corresponding to the (002) facet of graphite (Fig. S14b, SI). The XRD pattern was consistent throughout the three stages of the imprinting process.

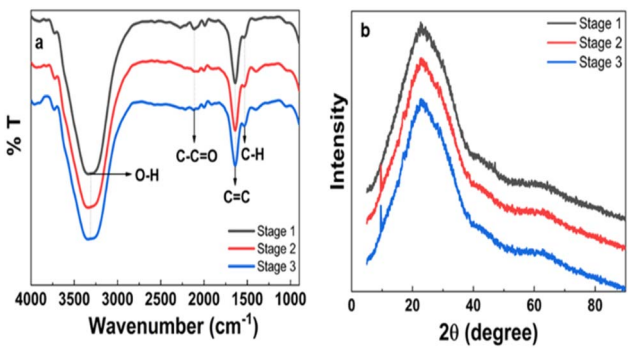

Fig. 9 (a) FT-IR spectrum, and (b) XRD plot of the CDs at various stages.

Raman spectroscopy was employed to investigate the structural characteristics and defect states of CDs. As presented in Fig. S14c, SI, the Raman spectrum of PSS-Cd-CDs displayed two distinct peaks at 1363.82 cm^{-1} and 1532.91 cm^{-1}. The D bands, often referred to as the disorder band, appeared at 1363.82 cm^{-1} and originates from the first-order Raman scattering process. The graphitic or G bands which appeared at 1532.91 cm^{-1}, are associated with the doubly degenerate phonon mode. These bands indicate the defects, disorder, and the crystallinity of PSS-Cd-CDs.[40] The I_D/I_G ratio of 3.868 indicates a high level of structural defects, which can be attributed to the abundant functional groups present on the surface of PSS-Cd-CDs. In contrast, the characteristic D and G bands are absent in the Raman spectrum of PSS, and the Raman peaks observed for PSS do not appear in the spectrum of PSS-Cd-CDs. This confirms that PSS-Cd-CDs are free from unreacted PSS fragments, indicating the successful synthesis of PSS-Cd-CDs.

The ^{1}H NMR spectrum of the PSS-Cd-CDs showed a clear difference from that of PSS. The multiplets observed for aromatic protons and sharp peaks of PSS are largely absent in the ^{1}H NMR spectrum of PSS-Cd-CDs. The spectrum of PSS-Cd-CDs was found to be broadened, with low-intensity signals and several downfield resonances. PSS possesses aliphatic protons observed at 0–2 ppm and the disappearance of these peaks in CDs indicated the decomposition of the polymer backbone during CD formation (Fig. S15, SI). Broad signals in the 3–6 ppm region were consistent with protons on oxygenated aliphatic carbons and reflect the high heterogeneity of surface environments on the PSS-Cd-CDs. The broadening of aromatic peaks at 6–8 ppm supports decomposition or carbonization of the styrene rings during CD formation and the formation of amorphous sp^2/sp^3 carbon domains. The appearance of broad, de-shielded resonances at far downfield positions (10–13 ppm) indicated the presence of carboxylic acids on the PSS-Cd-CDs surface. Overall, the ^{1}H NMR data validate the structural conversion of PSS into PSS-derived carbon dots with abundant oxygenated surface functionalities that are responsible for the observed broad and downfield NMR features.[41,42]

During the sensing process, Cd(II) ions are effectively captured by CDs of Stage 2 due to specific recognition sites and coordinate bond interactions with functional groups present on the surface of Stage 2 CDs. The UV-visible absorption spectrum of Stage 2 CDs exhibited peaks at 220 nm and 260 nm, which are associated with π–π* transitions of the conjugated C=C bond and n–π* transitions of the C=O bonds. In the PL spectra, CDs of Stage 2 showed excitation wavelength-dependent emissions, when excited at different wavelengths ranging from 220 to 400 nm, taken at an interval of 20 nm. The maximum emission (λ_{max}) was found at 315 nm when the Stage2 CDs are excited at

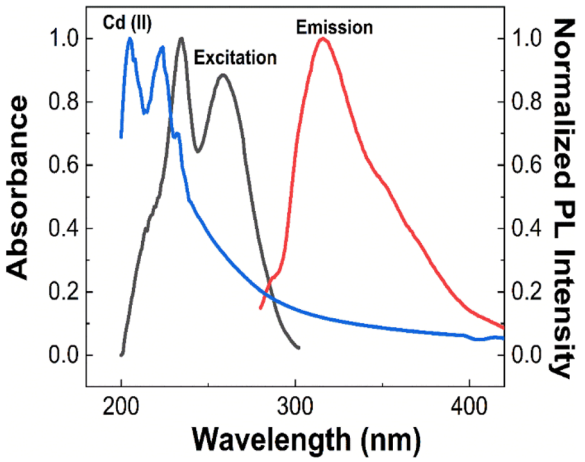

Fig. 10 The UV-visible absorption spectrum of Cd(II) ions (blue line), excitation spectrum (emission recorded at 315 nm) (black line), and emission spectrum (λ_{ex} = 260 nm) (red line) of Stage 2 CDs, respectively.

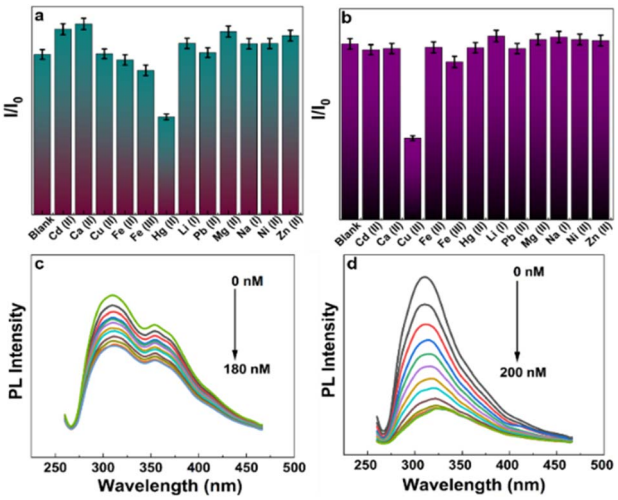

Fig. 11 (a) The PL intensity at 315 nm of PSS-Hg-CDs with binding sites to different metal ions, (b) the PL intensity at 315 nm of PSS-Cu-CDs with binding sites to various metal ions, (c) the PL spectra of PSS-Hg-CDs with binding sites exposed to different concentrations of Hg(II) (λ_{ex} = 260 nm), and (d) the PL spectra of PSS-Cu-CDs with binding sites dispersed in varying concentrations of Cu(II) (λ_{ex} = 260 nm).

a wavelength of 260 nm. For the inner filter effect to be effective, there must be significant overlap between the Cd(II) ions absorption band and the excitation and/or emission bands of the CDs of Stage 2. As shown in Fig. 10, the absorption band of Cd(II) ions was centered at 204 nm and 223 nm with a shoulder peak at 235 nm, while the excitation spectrum of Stage 2 CDs was located at 233 nm and 260 nm, with its emission spectra centered at 315 nm when excited at 260 nm. Fig. 10 clearly shows the spectral overlap of the absorption bands of Cd(II) with the excitation bands of Stage 2 CDs, giving rise to the inner filter effect,[43] a possible mechanism for the quenching of the PL intensity of Stage 2 CDs towards Cd ions.

3.3 Other systems

In order to examine the general applicability of our method, we chose to synthesize PSS-CDs tethered with Cu(II) and Hg(II) (denoted as PSS-Cu-CDs, and PSS-Hg-CDs, respectively) other than PSS-Cd-CDs, and analysed their fluorescence responses (Fig. 11). The Cu(II) ions and the Hg(II) ions were removed from the surfaces of PSS-Cu-CDs and PSS-Hg-CDs using NaOH, creating PSS-Cu-CDs and PSS-Hg-CDs with the binding sites. PSS-Cu-CDs and PSS-Hg-CDs with the binding sites exhibited specificity in the fluorescence response (Fig. 11a and b).

The fluorescence response was found to be specific, which means when different metal ions were introduced to the dispersion of PSS-Cu-CDs with the binding sites, it showed selective fluorescence quenching towards Cu(II) ions, and a similar trend was observed for the PSS-Hg-CDs system. Both PSS-Cu-CDs and PSS-Hg-CDs with binding sites were found to be sensitive to the concentration of Cu(II) and Hg(II) ions (Fig. 11c and d). The reason for the specific adsorption of metal ions on the surfaces of CDs of Stage 2, where the binding sites are created is an intriguing question. The possibility of metal ions forming coordinate bonds with the oxygen-containing surface functionalities of the CDs is worth exploring. Coordinate bond formation by the metal ions depends on factors such as atomic number, ionic radius, coordination number, charge, and valence electrons.[22] In the case of PSS-Cd-CDs, the ionic radii corresponding to the coordination number of Cd(II) is not comparable with the atomically similar metal ions (Zn(II) and Hg(II)) (Table 6), so the size/shape of the recognition sites existing in CDs of Stage 2 for Cd(II) ions is not fit for Zn(II) and Hg(II). Other than Zn(II) and Hg(II) ions, the transition elements like (Cu(II), Fe(II), Fe(III), Pb(II), and Ni(II)), were considered as competitive ions in the selectivity studies of CDs of Stage 2. The interference of these ions was eliminated by the size/shape of the recognition sites. The interference of other cations such as (Ca(II), Na(I), Li(I), and Mg(II) can be neglected, since they have different charges and show huge differences in the ionic radii. Therefore, the PSS-Cd-CDs with the binding sites have a specific fluorescence response towards only Cd(II) ions. Since Cd(II) ions are toxic to human lives and the environment,[44] we intended to study the ion-imprinting characteristics of the PSS-Cd-CDs system in detail (Section 3.2).

3.4 Real water sample analysis

The Stage 2 CDs were employed for the selective and sensitive detection of Cd ions in real samples, such as tap water and lake water. The concentration of the Cd ions in the samples was below the detection limit of the proposed method, due to which different concentrations of Cd ions were spiked to the samples and used for fluorescent analysis. The spike recoveries for the quantitative determination of Cd ions in tap and lake water were performed using Stage 2 CDs by adding varying concentrations of Cd ions (10, 20, 30, 40, and 50 μM, respectively). The concentrations of Cd ions in the real samples were found (by linear fitting the plot of concentration of Cd ions *versus* the PL intensity (Fig. S16, SI)), and the results are presented in Table 7. The Cd ion detection in real samples ranged from 84.11% to 112.67% at five spiked concentrations. The relative standard

Table 6 Comparison of the atomic properties of the selected transition metals

Ions	Atomic number	Valence electrons	Charge	Ionic radius	Coordination number
Zn(II)	30	$3d^{10}\ 4s^2$	2	60	4
				74	6
				90	8
Cd(II)	48	$4d^{10}\ 5s^2$	2	78	4
				95	6
				110	8
				131	12
Hg(II)	80	$5d^{10}\ 6s^2$	2	69	2
				96	4
				102	6
				114	8
Fe(II)	26	$3d^6\ 4s^2$	2	49	4
				55	6
				78	8
Cu(II)	29	$3d^{10}\ 4s^1$	2	57	4
				73	6
Pb(II)	82	$6s^2\ 6p^2$	2	119	6
				129	8
				140	10
				149	12
Ni(II)	28	$3d^8\ 4s^2$	2	63	4
				83	6

Table 7 Results of determination of Cd(II) ions in real samples

Sl no.	Samples	[a]Added (μM)	Found (μM)	Recovery (%)	RSD (%, $n = 3$)
1	Lake water	0	—	—	—
		10	8.41	84.11	1.44
		20	19.53	97.63	1.48
		30	33.81	112.67	1.53
		40	40.15	100.40	1.56
		50	48.09	96.19	1.59
2	Tap water	0	—	—	—
		10	10.71	107.14	0.86
		20	17.86	89.30	0.87
		30	32.15	107.16	0.89
		40	39.27	98.17	0.90
		50	50.01	100.02	0.91

[a] This represents the concentration of 20 μL of Cd(II) solution added to the 3 mL of the samples.

deviations (RSD) varied between 0.86% and 1.59%. This indicates the sensor has good accuracy and can be used for the detection of Cd(II) ions in the real samples.

4. Conclusions

A novel method for the usage of CDs as rationally designed sensitive fluorescent nanoprobe to detect the presence of Cd(II) ions in aqueous solutions is developed. A polyelectrolyte (PSS) modified with Cd(II) ions was used for the customized synthesis of CDs. This strategy incorporates Cd(II) ions on the CDs produced. An ion-imprinting based strategy is used for the use of these CDs as fluorescent probes. The ion-imprinting approach outlined here involves three key steps, each analysed through fluorescence response. By considering the benefits of CDs, ion-imprinting techniques, and fluorescence spectroscopy, the system and method developed through this work demonstrate a novel and simple approach for highly selective detection of Cd(II) ions. We validated the effectiveness of this method by systematically detecting Cd(II) ions with a detection limit (LOD) of 3.62 nM. Remarkably, this method eliminates the requirement for complex pre-treatment steps for the sensing of cadmium ions. In summary, the sensor developed in this study serves as a promising alternative to existing methods, providing a sensitive, rapid, and highly selective platform for detecting target analytes. The selective detection is due to the coordination of Cd(II) with the oxygen-containing groups on the Stage 2 CDs surface. The strategy presented here represents a conceptual advancement in the use of CDs as sensors. This could be used as a generic pathway for the utilization of CDs as fluorescent probes.

Author contributions

Aishwarya Joji Mathew: conceptualization, methodology, investigation, data curation, formal analysis, software, visualization, validation and writing – original draft, writing – review & editing. Vinod T. P.: conceptualization, investigation, formal analysis, software, visualization, validation, resources, writing – original draft, writing – review & editing, funding acquisition and project administration and supervision. Yamuna Nair: methodology, funding acquisition and project administration.

Conflicts of interest

The authors declare that they have no known competing financial interests or personal relationships that could have appeared to influence the work reported in this paper.

Data availability

The data supporting this article have been included as part of the supplementary information (SI). Supplementary information is available. See DOI: https://doi.org/10.1039/d5na00892a.

Acknowledgements

Aishwarya Joji Mathew is grateful to Christ University for the research fellowship. Vinod T. P. is thankful to Centre for Research Projects (CRP), Christ University, for the Seed Money Grant SMSS-2334. The authors are thankful to Vision Group on Science and Technology (VGST), Govt. of Karnataka, for the K-FIST-L1 grant (GRD No. 1143).

References

1 G. Ayiloor Rajesh, V. L. John, A. Pookunnath Santhosh, A. Krishnan Nair Ambika and V. Thavarool Puthiyedath, *Part. Part. Syst. Charact.*, 2022, **39**, 1–23.
2 D. Ozyurt, M. Al Kobaisi, R. K. Hocking and B. Fox, *Carbon Trends*, 2023, **12**, 100276.
3 V. L. John, A. R. Nayana, T. R. Keerthi, A. K. K A, B. C. P. Sasidharan and V. T P, *Macromol. Biosci.*, 2023, **23**, 2300081.
4 V. Lisa John, F. P M, C. K P and V. T P, *Nanotechnology*, 2022, **33**, 495706.
5 M. Sharma, N. Mazumder, P. M. Ajayan and P. Deb, *J. Phys.:Condens. Matter*, 2024, **36**, 283001.
6 L. Wang, W. Li, L. Yin, Y. Liu, H. Guo, J. Lai, Y. Han, G. Li, M. Li, J. Zhang, R. Vajtai, P. M. Ajayan and M. Wu, *Sci. Adv.*, 2020, **6**, 33008913.
7 V. V. T N, A. S. Mathew, D. Mathew, J. Mathew and R. E K, *Prep. Biochem. Biotechnol.*, 2025, 1–14.
8 S. Nandi, S. Kolusheva, R. Malishev, A. Trachtenberg, T. P. Vinod and R. Jelinek, *Chem.–Eur. J.*, 2015, **21**, 7755–7759.
9 G. Kandasamy, *C*, 2019, **5**, 24.
10 S. Nandi, M. Ritenberg and R. Jelinek, *Analyst*, 2015, **140**, 4232–4237.
11 S. Cui, Y. Wu, Y. Liu, Q. Guan, Y. Zhang, Y. Zhang, S. Luo, M. Xu and J. Wang, *Chin. Chem. Lett.*, 2020, **31**, 487–493.
12 S. Mohandoss, N. Ahmad, M. R. Khan, K. S. Velu, S. Palanisamy, S. You, A. J. Kumar and Y. R. Lee, *Environ. Res.*, 2023, **228**, 115898.
13 K. K. Rao and B. Prakash, *ACS Sens.*, 2025, **10**, 3423–3432.
14 R. Madhuri, E. Roy, K. Gupta and P. K. Sharma, *Combination of Molecular Imprinting and Nanotechnology: Beginning of a New Horizon*, Wiley Blackwell, 2014, 9781118773, pp. 367–422.
15 J. Fu, L. Chen, J. Li and Z. Zhang, *J. Mater. Chem. A*, 2015, **3**, 13598–13627.
16 X. Sun, M. Jiang, L. Chen and N. Niu, *Microchim. Acta*, 2021, **188**, 297.
17 L. Chen, Y. Lu, M. Qin, F. Liu, L. Huang, J. Wang, H. Xu, N. Li, G. Huang, Z. Luo and B. Zheng, *Sensors*, 2020, **20**, 995.
18 J. Wang, C. Jiang, X. Wang, L. Wang, A. Chen, J. Hu and Z. Luo, *Analyst*, 2016, **141**, 5886–5892.
19 Z. Wang, C. Zhou, S. Wu and C. Sun, *Polymers*, 2021, **13**, 1376.
20 Q. Bai, C. Huang, S. Ma, B. Gong and J. Ou, *Sep. Purif. Technol.*, 2023, **315**, 123666.
21 V. Lisa John, F. Joy, A. Jose Kollannoor, K. Joseph, Y. Nair and V. T P, *J. Colloid Interface Sci.*, 2022, **617**, 730–744.
22 H. Lu, S. Xu and J. Liu, *ACS Sens.*, 2019, **4**, 1917–1924.
23 G. Kuppuraj, M. Dudev and C. Lim, *J. Phys. Chem. B*, 2009, **113**, 2952–2960.
24 A. Kumar, S. Asu, P. Mukherjee, P. Singh, A. Kumari and S. K. Sahu, *J. Photochem. Photobiol., A*, 2021, **406**, 113019.
25 K. J. Mintz, M. Bartoli, M. Rovere, Y. Zhou, S. D. Hettiarachchi, S. Paudyal, J. Chen, J. B. Domena, P. Y. Liyanage, R. Sampson, D. Khadka, R. R. Pandey, S. Huang, C. C. Chusuei, A. Tagliaferro and R. M. Leblanc, *Carbon.*, 2021, **173**, 433–447.
26 J. Kim, H. J. Shim, J. Yang, M. K. Choi, D. C. Kim, J. Kim, T. Hyeon and D. Kim, *Adv. Mater.*, 2017, **29**, 1700217.
27 B. Zhu, S. Sun, Y. Wang, S. Deng, G. Qian, M. Wang and A. Hu, *J. Mater. Chem. C*, 2013, **1**, 580–586.
28 J. Cheng, C.-F. Wang, Y. Zhang, S. Yang and S. Chen, *RSC Adv.*, 2016, **6**, 37189–37194.
29 J. Xu, C. Wang, H. Li and W. Zhao, *RSC Adv.*, 2020, **10**, 2536–2544.
30 M. Masteri-Farahani, S. Mashhadi-Ramezani and N. Mosleh, *Spectrochim. Acta, Part A*, 2020, **229**, 118021.
31 S. Bhogal, I. Mohiuddin, S. Kumar, A. K. Malik, K.-H. Kim and K. Kaur, *Sci. Total Environ.*, 2022, **847**, 157356.
32 X. Zhou, X. Gao, M. Liu, C. Wang and F. Chu, *Microchim. Acta*, 2017, **184**, 4175–4181.
33 S. P. S and S. S R, *RSC Adv.*, 2024, **14**, 17471–17479.
34 X. Zhou, X. Gao, M. Liu, C. Wang and F. Chu, *Microchim. Acta*, 2017, **184**, 4175–4181.
35 P. Pansari, G. Durga and R. Javed, *Chem. Pap.*, 2024, **78**, 5993–6010.
36 K. G. Nguyen, I.-A. Baragau, R. Gromicova, A. Nicolaev, S. A. J. Thomson, A. Rennie, N. P. Power, M. T. Sajjad and S. Kellici, *Sci. Rep.*, 2022, **12**, 13806.
37 S. S. Jones, P. Sahatiya and S. Badhulika, *New J. Chem.*, 2017, **41**, 13130–13139.
38 J. Ge, Q. Jia, W. Liu, M. Lan, B. Zhou, L. Guo, H. Zhou, H. Zhang, Y. Wang, Y. Gu, X. Meng and P. Wang, *Adv. Healthc. Mater.*, 2016, **5**, 665–675.
39 F. Du, L. Zhang, L. Zhang, M. Zhang, A. Gong, Y. Tan, J. Miao, Y. Gong, M. Sun, H. Ju, C. Wu and S. Zou, *Biomaterials*, 2017, **121**, 109–120.
40 L. M. Malard, M. A. Pimenta, G. Dresselhaus and M. S. Dresselhaus, *Phys. Rep.*, 2009, **473**, 51–87.
41 L. Yuan, M. Yan, X. Tao, X. Yang, W. Long, W. Xia, H. Liao, Y. Gong, K. Zhang, Z. Xia and Q. Fu, *Carbon.*, 2024, **226**, 119169.
42 Y. Gong, D. Wang, P. Chen, R. Deng, M. Yan, B. Ji, L. Liu, X. Tao, Z. Xia and Q. Fu, *Food Chem.*, 2025, **493**, 146088.
43 M. Zheng, Z. Xie, D. Qu, D. Li, P. Du, X. Jing and Z. Sun, *ACS Appl. Mater. Interfaces*, 2013, **5**, 13242–13247.
44 M. A. Irshad, R. Nawaz, E. Wojciechowska, M. Mohsin, N. Nawrot, I. Nasim and F. Hussain, *Water, Air, Soil Pollut.*, 2023, **234**, 54.